Oral Diseases (2005) 11, 35–43

http://www.blackwellmunksgaard.com

Radiology

Utility of three dimension fast asymmetric spin-echo (3D-FASE) sequences in MR sialographic sequences: model and volunteer studies

Y Morimoto[1], T Tanaka[1], S Kito[1], K Tominaga[2], I Yoshioka[2], Y Yamashita[3], T Shibuya[3], Y Matsufuji[4], M Kodama[2], T Takahashi[3], J Fukuda[2], T Ohba[1]

[1]*Department of Dental Radiology, Kyushu Dental College, Kokurakita-ku, Kitakyushu, Japan;* [2]*1st Department of Oral and Maxillofacial Surgery, Kyushu Dental College, Kokurakita-ku, Kitakyushu, Japan;* [3]*2nd Department of Oral and Maxillofacial Surgery, Kyushu Dental College, Kokurakita-ku, Kitakyushu, Japan;* [4]*Toshiba Medical Co., Sukukita, Kasuga, Fukuoka, Japan*

OBJECTIVES: To evaluate the utility of 3D-FASE for the visualization of salivary gland ducts for use in MR sialographic sequences.
METHODS: We compared MR sialographic images and virtual endoscopic views from 3D-FASE with those from three kinds of sequences described by previous reports in a 3D parotid gland duct model and volunteer. The four sequences were two-dimension fast spin-echo (2D-FSE), three-dimension fast spin-echo (3D-FSE), two-dimension fast asymmetric spin-echo (2D-FASE), and three-dimension fast asymmetric spin-echo (3D-FASE).
RESULTS: In the 3D parotid gland duct model, image visibility on visual score was clearest with 3D-FSE, followed by 3D-FASE ($P = 0.028$). In the volunteers, the visualization of images improved in the following order: 3D-FASE > 3D-FSE > 2D-FSE > 2D-FASE.
CONCLUSIONS: The technique of 3D-FASE sequencing is more suitable and useful for MR sialography with an appropriate acquisition time.
Oral Diseases (2005) **11**, 35–43

Keywords: 3D-FASE sequences; magnetic resonance sialography; salivary glands; virtual endoscopy

Introduction

Magnetic resonance (MR) imaging is widely used in examinations of the salivary glands (Mandelblatt *et al*, 1987; Teresi *et al*, 1987a,b; Hebert *et al*, 1993; Thibauly *et al*, 1993; Lomas *et al*, 1996, 1996; Fischbach *et al*, 1997; Murakami *et al*, 1998; Varghese *et al*, 1999; Becker *et al*, 2000; Jager *et al*, 2000; Shojaku *et al*, 2000; Yousem *et al*, 2000; Sakamoto *et al*, 2001; Morimoto *et al*, 2002, in press). One form of this imaging, MR sialography, was first developed by Lomas et al. and is a completely non-invasive technique, unlike X-ray sialography, for examining salivary gland ducts (Lomas *et al*, 1996; Fischbach *et al*, 1997; Murakami *et al*, 1998; Varghese *et al*, 1999; Becker *et al*, 2000; Jager *et al*, 2000; Shojaku *et al*, 2000; Yousem *et al*, 2000; Sakamoto *et al*, 2001; Morimoto *et al*, 2002, in press). Initially, the sequencing of the application for MR sialography used heavily T2-weighted rapid acquisition with relaxation enhancement (RARE). Recently, MR sialography has been reportedly obtained with a short acquisition time through the Fourier half-range acquisition single-shot turbo spin-echo (HASTE) technique, developed by Murakami *et al* (1998).

Fast asymmetric spin-echo (FASE) sequencing is similar to HASTE sequencing (Yang *et al*, 1999; Naganawa *et al*, 2001; Morimoto *et al*, 2002, in press). One of the advantages of FASE sequencing is its ability to excite a three-dimensional (3D) sample from one slab (Yang *et al*, 1999; Naganawa *et al*, 2001; Morimoto *et al*, 2002, in press), and the slice thickness can be decreased to as little as 0.5 mm. A decrease in slice thickness of this magnitude should produce a marked improvement in spatial resolution (Yang *et al*, 1999; Becker *et al*, 2000; Naganawa *et al*, 2001; Morimoto *et al*, 2002, in press). As a result, the 3D-sequences are easily applied for the evaluation of the inner ear (Yang *et al*, 1999) and MR sialography (Becker *et al*, 2000; Morimoto *et al*, 2002, in press). Images obtained using MR sialography with 3D-FASE sequencing promise to be of a higher quality than those obtained using other sequences (Becker *et al*, 2000; Morimoto *et al*, 2002, in press). However, to our knowledge, the most suitable sequence for MR sialography is 2D-turbo spin echo

Correspondence: Yasuhiro Morimoto, Department of Dental Radiology, Kyushu Dental College, 2-6-1 Manazuru, Kokurakita-ku, Kitakyushu 803-8580, Japan. Tel: 81-93-582-1131 (ext. 2116, 1331), Fax: 81-93-581-2152, E-mail: rad-mori@kyu-dent.ac.jp
Received 1 October 2003; revised 29 February 2004 and 20 May 2004; accepted 28 May 2004

(TSE) as reported by Sakamoto *et al* (2001), without including 3D-sequences.

MR virtual endoscopic views use well-known techniques, such as perspective volume-rendering, fly-through means, and interactive visualization (Davis *et al*, 1996; Neri *et al*, 1997); we combined these techniques with MR sialography to create a new imaging approach for parotid gland ducts (Morimoto *et al*, 2002, in press). Endoscopic viewing using MR sialographic data sets is a very attractive tool for observation of the endoluminal anatomy of the parotid gland ducts and for visualizing any pathological changes.

In the present study, we compared MR sialographic images from 3D-FASE sequences with those from three other sequences described in previous reports in order to examine the advantages of this technique in terms of resolution and acquisition time in a 3D parotid gland duct model and volunteer patients. Producibility of the virtual endoscopic views was used as a parameter to judge the quality of the MR sialographic images with four different sequences.

Materials and methods

All images were acquired using a 1.5-T full-body MR system (VISART; Toshiba, Fukuoka, Japan) with a circular polarized neck coil to visualize the parotid gland ducts (Morimoto *et al*, 2002, in press; Tanaka *et al*, 2002). In the same session in which conventional MR studies of the parotid glands were obtained, MR sialography was performed using four different sequences including 3D-FASE (Table 1). The acquisition time of the four sequences was decided based on the signal to noise ratio (SNR) from four relative sequences, which was found to be an appropriate level by preliminary phantom study (Irie *et al*, 1998; Sakamoto *et al*, 2001). A 3D model representing the parotid gland was constructed. As the superficial part of the real parotid gland lies beneath the fatty tissue of the face, and because the gland contains ducts of various diameters, the phantom consisted of five sizes of polyethylene tubing including the water with internal diameters of 2.00 mm (A), 1.50 mm (B), 1.00 mm (C), 0.76 mm (D and E), and 0.50 mm (F) against an oil background. The SNR between the distilled water in the polyethylene tubes and the surrounding solution was measured for each MR sequence. The signal intensity in each region of interest (ROI) was measured from the image of the distilled water in the polyethylene tube and the surrounding solution, and the SNR were determined as follows: SNR = [signal of the polyethylene tube/standard deviation (s.d.) air] $\times \sqrt{2}$. The thinnest possible slice thickness for MR sialography using relative sequence was used for the clinical studies. In the 2D-sequences, both single-section acquisition with thick sections (SS) as 30 mm and sequential multi-section imaging (MS) with thin sections as 1.5 (in FSE) or 2.2 (in FASE) mm followed by maximum intensity projection (MIP) reconstruction were used. For 2D-sequences using sequential MS with thin sections followed by MIP reconstruction, no intersection gap was set according to Irie *et al* (1998). In addition, a slice thickness of 1.5 mm was used for the volunteer study using the 3D-FSE sequences, rather than the 0.5 mm thickness used for the phantom study. The reason is that it took over 1 h to acquire MR images when the slice thickness was 0.5 mm. For all sequences, fat saturation suppressed the signals from the subcutaneous fat during MR sialography.

Table 1 Imaging parameters

Sequence	*TR/TE/FA/ETL*	*Thickness (mm)*	*Matrix*	*Acquisition time (min:s)*	*FOV (mm)*
2D-FSE	6000/254/90/37	1.5	512 × 512	5:24	250 × 250
		30	512 × 512	2:42	250 × 250
3D-FSE	6000/250/90/27	0.5	512 × 512	118:54	250 × 250
		1.5	512 × 512	39:42	250 × 250
2D-FASE	6000/250/90/148	2.2	512 × 512	2:30	250 × 250
		30	512 × 512	2:30	250 × 250
3D-FASE	6000/250/90/148	0.5	512 × 512	13:18	250 × 250
		1.5	512 × 512	4:32	250 × 250

The parotid gland ducts were identified on an initial set of routine T2-weighted axial images and an oblique sagittal acquisition was used to capture an image of the parotid gland ducts. Postprocessing of the MR sialographic images was performed with MIP reconstructions except for the single-section acquisition with thick sections of 2D-sequences. The MR sialographic images from the four sequences were compared according to the quality of the MIP reformatted-acquisition. The MR data sets were transferred to a workstation, into which Navigator software (GE/Medical Systems, Milwaukee, WI, USA) was installed for production of MR virtual endoscopic views except for the single-section acquisition with thick sections of 2D-sequences.

The imaging parameters and methods of MR virtual endoscopy for salivary gland ducts were as described in Morimoto *et al* (2002, in press). Endoscopic views from the MR sialography data sets using the four kinds of sequencing were generated with Navigator software, which displays internal views by surface-rendering anatomical structures with simulated highlighting and shading. After an image data set was loaded, the endoscopic view was presented on the screen. When setting the threshold level, either a 'black in white' or 'white in black' paradigm was chosen. For all four different sequencing data sets, we chose the 'white in black' paradigm, because the duct spaces of the parotid gland appear as a high intensity area on the MR sialographic images. We set the threshold level to be between 250 and 800 units to 1000 units, depending on the case. In the 'white in black' paradigm, all pixels above the threshold level were considered to be within the ducts.

The method used for evaluation of the MR sialographic images with the four sequences was a slightly modified version of that described in Irie *et al* (1998) and Sakamoto *et al* (2001).

First, for subjective analysis, MR sialographic images of the model parotid gland ducts obtained using the four

sequences were assessed by two experimental radiologists (Y.M. and T.T.) operating in consensus on visualization of the tubes. The source and MIP images from each sequence were analyzed. The degree of conspicuity of the tube was evaluated, and was graded from 0 to 3: grade 0, difficult to detect on the source image; grade 1, detectable on the source image although difficult to detect on the MIP image; grade 2, mostly detectable on the MIP image; and grade 3, wholly detectable on the MIP image. MR sialographic images of the model parotid gland ducts were obtained five times with repositioning of the phantom. The minimum tube diameters were determined using respective sequences by consensus of the two radiologists, and were subsequently measured using the scanner-computer analysis system. In the model images obtained using each sequence, MR images of the water column in each tube were digitized using a GT9500 scanner (Epson, Tokyo, Japan) connected to a Power Macintosh G4/350 computer (Apple Computer, Cupertiro, CA, USA). Images were analyzed using NIH Image, version 1.61 (courtesy of Wayne Rasband, National Institutes of Health, Bethesda, MD, USA). The ratio between the width of the water-column image and the actual internal diameter of the tube was then calculated for each of the five images. In addition, the thinnest tubes of producibility for MR virtual endoscopic views for the best image of five were identified from among the four sequences. For objective analysis, duct signal intensity and the corresponding background signal intensity in the phase-encoding direction were measured on the console, and the contrast-to-noise ratio (C/N) was calculated as tube signal intensity minus background signal intensity divided by noise. Noise was defined as the standard deviation of the background signal intensity.

Next, we recruited 15 volunteers (nine men and six women, aged 18–62 years; mean $\pm$ s.d. = 29.7 $\pm$ 9.24) with no salivary gland pathology, as confirmed by history and clinical examination. Informed consent was obtained from all volunteers prior to the MR examination. For the subjective analysis, MR sialographic images (both of the source and MIP images) of the left side parotid gland ducts obtained using the four sequences were assessed by the same radiologists operating in consensus on visualization of the main duct and the peripheral ducts (secondary and tertiary branches), each being scored as one of the previously defined grades. Furthermore, we also judged the advantages of sequences based on producibility of visualization completely throughout the main duct in the virtual endoscopic views, which could be produced from all four sequences. The method of evaluating the utility of the MR virtual endoscopy in the four sequences was to compare the number of producible cases throughout the main parotid duct. As an objective analysis, parotid gland duct signal intensity and the corresponding background signal intensity in the phase-encoding direction were measured on the console, and C/N was calculated.

All results are expressed as mean $\pm$ s.e.m. In both the phantom and volunteer studies, various different visual scores, ratio width, SNR, and C/N were analyzed by ANOVA by SPSS ver. 11 (SPSS Inc., Chicago, IL, USA) for determination of the most suitable sequences for MR sialography. The acceptable level of significance was $P < 0.05$.

Results

Phantom study

The MR sialographic images and visual scores of the phantom model obtained by respective sequence are shown in Figure 1 and Table 2. With decreasing tube diameter, MR imaging quality with 3D-sequences was significantly better than that with 2D-sequences ($P < 0.0001$). In the 3D-sequences, the MR images of the tube were significantly superior with FSE than with FASE ($P = 0.028$), in the 2D-sequences ($P = 0.0018$). In terms of slice thickness, better images were obtained using a 0.5-mm slice thickness than with a 1.5-mm slice thickness when using 3D-FSE significantly ($P = 0.041$), but the opposite was true for 3D-FASE significantly ($P = 0.049$).

In the 2D-sequences, poorer images of the tube were obtained using sequential MS with thin sections followed by MIP reconstruction than when using single-section acquisition with thick sections (SS) significantly ($P < 0.0001$). The 0.5 mm tube was visualized on MR images using 3D-sequences, but not when using 2D-sequences. In the 0.76 mm tube, imaging quality for the various sequences were produced according to the following breakdown: 3D-FSE (0.5 mm) > 3D-FSE (1.5 mm) > 3D-FASE (1.5 mm) > 3D-FASE (0.5 mm) > 2D-FSE (SS) > 2D-FASE (SS) > 2D-FSE (MS) > 2D-FASE (MS) (Figure 2).

The ratio between the diameter of the tube on MR images and actual tube diameter are shown in Table 3. The 3D-sequences with 1.5 mm slice thickness appeared slightly magnified relative to that with 0.5 mm. The degree of magnification of diameter in all tubes using 3D-FASE MR sialographic images both of 1.5 and 0.5 mm slice thickness was significantly larger than using 3D-FSE ($P = 0.00034$), but not 2D-sequences. The degree of magnification and reduction of diameter in tubes using 2D-MS sequences was significantly larger than those using 3D-sequences ($P < 0.0001$). In the 2D-sequences with SS, all tubes showed a significant reduction in diameter, with this value differing widely from 1.

A comparison of the thinnest width of tubes in terms of producibility of virtual endoscopy with the MR data sets from four kinds of sequences is shown in Table 4. The following breakdown was obtained; 2D-FASE (MS) > 2D-FSE (MS) > 3D-FASE (0.5 mm slice thickness) = 3D-FASE (1.5 mm slice thickness) = 3D-FSE (1.5 mm slice thickness) > 3D-FSE (0.5 mm slice thickness). In both 2D-sequences with single thick slice methods, MR virtual endoscopy could not be obtained because of the limitations inherent with the 2D-data.

The mean C/Ns for the four sequences in the phantom study are shown in Table 5. The mean C/Ns using 3D-sequences was significantly greater than that using

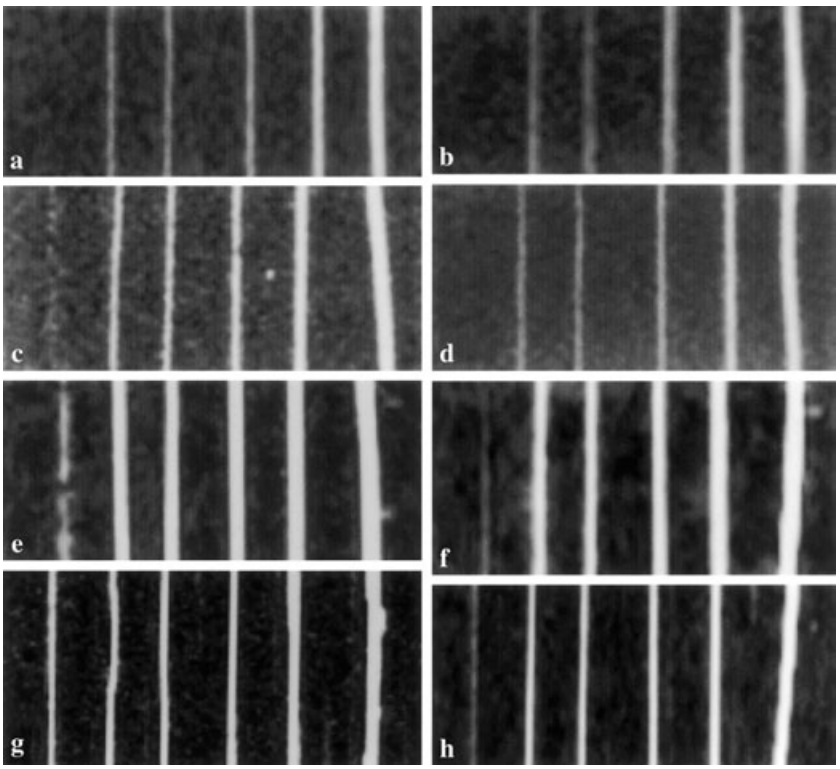

Figure 1 MR sialographic images of the phantom obtained using the four sequences: (a) 2D-FASE (MS), (b) 2D-FASE (SS), (c) 2D-FSE (MS), (d) 2D-FSE (SS), (e) 3D-FASE (slice thickness 0.5 mm), (f) 3D-FASE (1.5 mm), (g) 3D-FSE (0.5 mm), (h) 3D-FSE (1.5 mm). The image with 3D-FSE sequence (0.5, and 1.5 mm) provided the highest resolution image and the most accurate length of the width of water in each polyethylene tube. Second was with 3D-FASE (1.5 mm).

Table 2 Visual score for conspicuity of salivary gland duct's phantom with four different MR sequences

	Tube diameter				
	2.00	*1.50*	*1.00*	*0.76*	*0.50*
3D-FASE (0.5 mm)	3.0	3.0	2.6	2.2	1.4
3D-FASE (1.5 mm)	3.0	3.0	2.8	2.4	1.6
3D-FSE (0.5 mm)	3.0	3.0	3.0	2.6	1.8
3D-FSE (1.5 mm)	3.0	3.0	2.8	2.4	1.6
2D-FASE (SS)	2.8	2.6	2.0	1.6	0.2
2D-FASE (MS)	2.6	2.0	1.8	1.4	0.2
2D-FSE (SS)	3.0	2.8	2.2	1.8	0.6
2D-FSE (MS)	2.8	2.2	1.8	1.6	0.4

$n = 5$ (mean).

2D-sequences ($P < 0.0001$). The mean C/Ns using FSE was significantly larger than that using FASE in the both 3D- and 2D-sequences ($P < 0.0001$). There was no statistically significant difference in the C/Ns for 0.5 and 1.5 mm section thickness in the 3D-sequences. In the 2D-sequences, there was a statistically significant difference in the C/Ns using SS than those using MS ($P = 0.0086$).

Volunteer study

The MR sialographic images and visual scores of the parotid gland ducts of volunteers obtained by respective sequence are shown in Figure 3 and Table 6. The Stenson duct was visible along its entire length using all four sequences. Secondary branches were seen using 3D-FSE (1.5 mm slice thickness) and 3D-FASE (1.5 and 0.5 mm), but not with 2D-FSE and 2D-FASE.

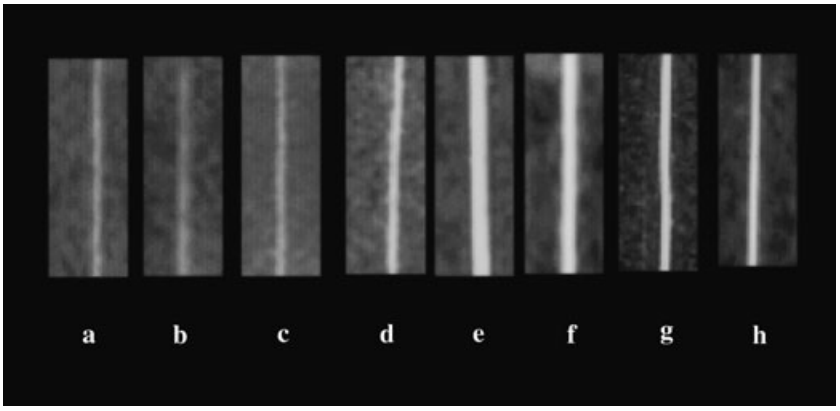

Figure 2 MR sialographic images of the phantom obtained using the four sequences in the 0.76 mm tube. (a) 2D-FASE (MS), (b) 2D-FASE (SS), (c) 2D-FSE (MS), (d) 2D-FSE (SS), (e) 3D-FASE (slice thickness 0.5 mm), (f) 3D-FASE (1.5 mm), (g) 3D-FSE (0.5 mm), (h) 3D-FSE (1.5 mm).

Table 3 Ratio of width of the MR image to actual diameter of the polyethylene tubes

	Tube diameter					
	2.00	*1.50*	*1.00*	*0.76*	*0.76*	*0.50*
3D-FASE	0.93	0.94	0.94	0.91	0.92	1.10
(0.5 mm) 3D-FASE	1.04	1.28	1.42	1.51	1.53	1.89
(1.5 mm) 3D-FSE	0.93	0.89	0.82	0.86	0.83	1.10
(0.5 mm) 3D-FSE	0.95	0.92	1.07	1.29	1.28	1.55
(1.5 mm) 2D-FASE (SS)	0.85	0.76	0.74	0.69	0.71	0.40
2D-FASE (MS)	1.11	1.13	1.27	1.43	1.51	–
2D-FSE (SS)	0.86	0.81	0.78	0.75	0.73	0.48
2D-FSE (MS)	1.07	1.10	1.35	1.45	1.48	–

$n = 5$ (mean).

Table 4 Diameters of producibihty completely throughout main ducts in MR virtual endoscopic views of tube with the four different sequences

Sequence	*Tube diameter*
3D-FASE (0.5 mm)	0.76 mm
3D-FASE (1.5 mm)	0.76 mm
3D-FASE (0.5 mm)	0.5 mm
3D-FASE (1.5 mm)	0.76 mm
2D-FASE (MS)	2.0 mm
2D-FSE (MS)	1.5 mm
2D-FSE	Not producible
FASE (SS)	Not producible

Table 5 Mean C/N at four different sequences in phantom study

	Tube diameter				
	2.00	*1.50*	*1.00*	*0.76*	*0.50*
3D-FASE (0.5 mm)	30.6	28.9	28.4	26.6	18.2
3D-FASE (1.5 mm)	31.2	27.8	27.9	26.2	19.4
3D-FSE (0.5 mm)	32.8	31.9	31.3	30.4	23.4
3D-FSE (1.5 mm)	39.5	33.7	32.4	29.8	21.8
2D-FASE (SS)	24.6	22.9	21.2	16.4	–
2D-FASE (MS)	20.7	17.5	13.1	18.1	–
2D-FSE (SS)	26.1	24.0	18.7	17.1	–
2D-FSE (MS)	24.9	22.5	21.3	19.5	–

$n = 5$ (mean).

However, the tertiary branch structure was only partially depicted in a few volunteers with both 3D-FSE and 3D-FASE (1.5 and 0.5 mm). The score of the main duct images is ranked in the following order: 3D-FASE (1.5 mm) > 3D-FASE (0.5 mm) > 3D-FSE > 2D-FSE (SS) > 2D-FASE (SS) > 2D-FASE (MS) > 2D-FSE (MS). A significant difference in visual score was found between 3D-FASE (1.5 mm) and 3D-FSE ($P = 0.048$), but not 3D-FASE (1.5 mm) and 3D-FASE (0.5 mm) or 3D-FASE (0.5 mm) and 3D-FSE. The score of secondary duct images is ranked in the following order: 3D-FASE (1.5 mm) > 3D-FASE (0.5 mm) > 3D-FSE > 2D-FSE (SS) > 2D-FASE (SS) > 2D-FSE (MS) > 2D-FASE (MS). A significant difference in visual score was found between 3D-FSE and 2D-FSE (SS) ($P = 0.041$). Furthermore, the tertiary duct score is ranked in the following order: 3D-FSE > 3D-FASE (1.5 mm) > 3D-FASE (0.5 mm) > 2D-FSE (SS) > 2D-FASE (SS) > 2D-FSE (MS) > 2D-FASE (MS). The number of producibility cases in MR virtual endoscopic views with 3D-FSE was 8, 9 with 3D-FASE (0.5 mm), 11 with 3D-FASE (1.5 mm), 1 with 2D-FSE (MS), and 0 with 2D-FASE (MS) (Table 7).

The mean C/Ns for the four sequences in the volunteer study are shown in Table 8. Results from the volunteer study were similar to those of the phantom. However, the mean C/Ns using 3D-FASE (1.5 mm) was significantly greater than that using 3D-FSE, which was consistent with the visual score in the volunteer study ($P = 0.026$).

Discussion

In the present study, we demonstrated that in MR sialography, 3D-FASE sequencing is a useful tool for improving resolution, even at an appropriate acquisition time, by comparing visualization among images obtained using four sequences described previously from a 3D parotid gland duct model and volunteers. If an acquisition time of over 30 min is used, 3D-FSE sequencing was capable of producing an excellent image in all four sequences. In the 2D-sequences, single-section acquisition with thick sections is more appropriate than sequential MS with thin sections followed by MIP for MR sialographic sequences. Furthermore, MR virtual endoscopic views of the parotid gland ducts were easily applied as evaluation methods of appropriate sequences for MR sialography.

In both the 3D parotid gland duct model and volunteer study, we selected four sequences including 3D-FASE in addition to previously described methods of MR sialography (Lomas *et al*, 1996; Fischbach *et al*, 1997; Murakami *et al*, 1998; Varghese *et al*, 1999; Becker *et al*, 2000; Jager *et al*, 2000; Shojaku *et al*, 2000; Yousem *et al*, 2000; Sakamoto *et al*, 2001; Morimoto *et al*, 2002, in press). 2D-FSE has been reported to be the most appropriate sequence for MR sialography by Sakamoto *et al* (2001). In their report, however, the most appropriate sequence for MR sialography sequences was not analyzed including 3D-excitation. Thus, we selected the 2D-FSE and 3D-FSE sequences in the present study. A disadvantage of 3D-excitation sequences is their duration, leading to motion artifacts. Therefore, 3D-FASE was also included (Becker *et al*, 2000; Morimoto *et al*, 2002, in press). Unfortunately, MR sialographic images obtained using 3D-CISS and 3D-SSFSE sequences were not possible using our current MR system. However, 3D-CISS sequences are based on gradient echo (GRE) methods, and in general 3D-CISS sequences have more disadvantages than 3D-FASE based on a comparative study in the head region (Naganawa *et al*, 2001). They can be more readily affected by changes in magnetization transfer induced by tissue adjacent to the nasal cavity and maxillary sinus in the head and neck than various sequences based on spin

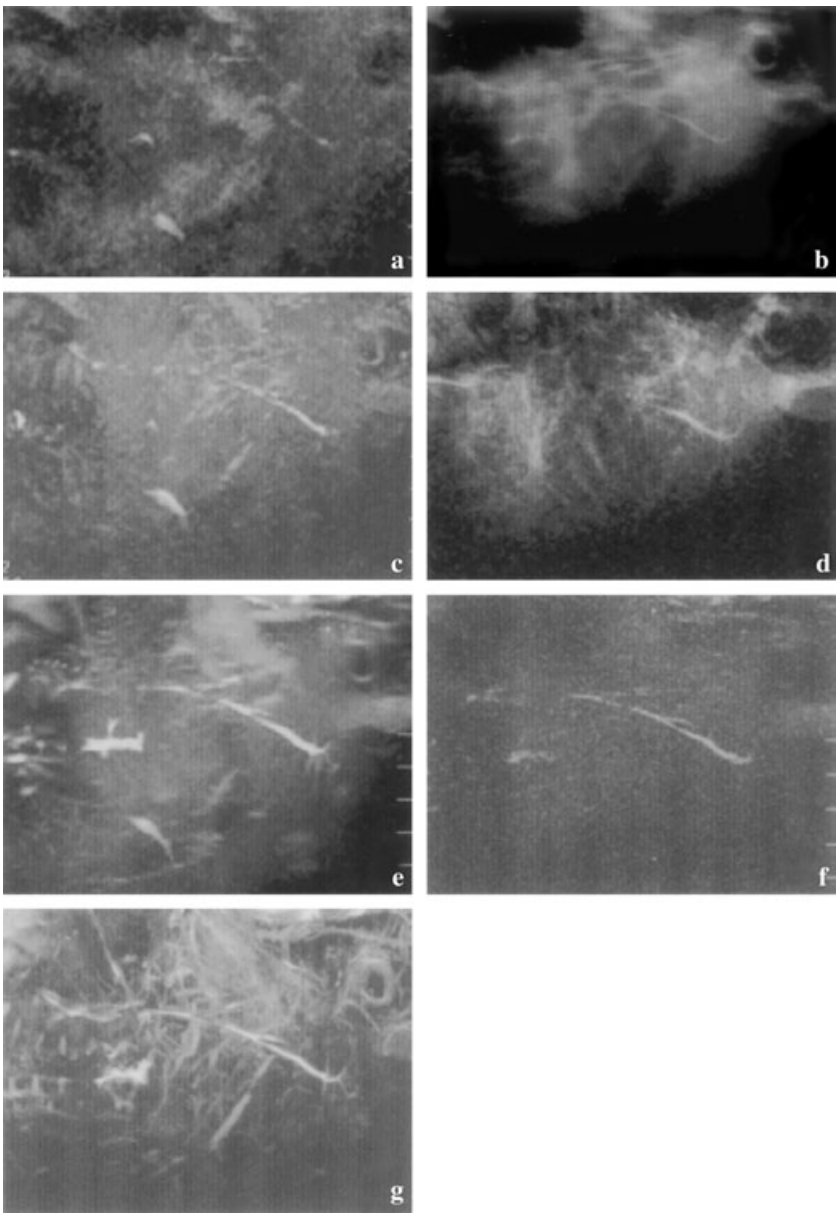

Figure 3 Sagittal oblique MR sialographic images of a 28-year-old healthy volunteer obtained using four sequences: (a) 2D-FASE (MS), (b) 2D-FASE (SS), (c) 2D-FSE (MS), (d) 2D-FSE (SS), (e) 3D-FASE (slice thickness 0.5 mm), (f) 3D-FASE (1.5 mm), (g) 3D-FSE (1.5 mm). The ducts were conspicuous with all sequences, and more visible with 3D-FASE sequences (1.5 mm).

Table 6 Visual scores for ducts in MR sialographic images of volunteers with the four different sequences

	Main ducts	*Secondary ducts*	*Tertiary ducts*
3D-FASE (0.5 mm)	2.40	1.00	0.33
3D-FASE (1.5 mm)	2.60	1.13	0.33
3D-FSE (1.5 mm)	2.27	0.93	0.40
2D-FASE (MS)	1.40	0.33	0
2D-FASE (SS)	1.80	0.47	0
2D-FSE (MS)	1.27	0.40	0
2D-FSE (SS)	1.93	0.53	0

$n = 15$ (mean).

Table 7 Numbers of producibihty completely throughout mam ducts in MR virtual endoscopic views of volunteers with the four different sequences

Sequences	*Numbers*
3D-FASE (0.5 mm)	9/15
3D-FASE (1.5 mm)	11/15
3D-FSE (1.5 mm)	8/15
2D-FASE (MS)	0/15
2D-FASE (SS)	1/15
2D-FSE (MS)	Not producible
2D-FSE (SS)	Not producible

echo methods. In addition, sequences cannot be obtained using fat suppression sequences. For the 3D-SSFSE sequences, the acquisition time is twice as long as the time using 3D-FASE, and movement artifacts are more common. Thus, we believe that the absence of 3D-CISS and -SSFSE sequences is not a limitation of the present study.

Table 8 Mean C/N at four different sequences in volunteer study

	Main ducts
3D-FASE (0.5 mm)	25.4
3D-FASE (1.5 mm)	31.5
3D-FSE (1.5 mm)	28.5
2D-FASE (SS)	23.2
2D-FASE (MS)	17.9
2D-FSE (SS)	23.2
2D-FSE (MS)	19.6

$n = 5$ (mean).

The diameters of polyethylene tube in the phantom study were decided based on previous reports where the mean diameter of parotid and submandibular gland ducts were found to range between 0.5 and 1.5 mm (Zenk *et al*, 1998a,b). Therefore, the pixel size also should be about 0.8×0.8 mm, and a matrix size of 512×512 was selected in the present study. Sakamoto *et al* (2001) also reported an appropriate matrix and pixel size for MR sialography of 512×512 and 0.8×0.8 mm, respectively. As to slice thickness, we selected 0.5 and 1.5 mm for 3D-sequences in the present study. A slice thickness of 0.5 mm, the thinnest possible slice, should be selected to evaluate the improvement of MR sialographic image quality, and 1.5 mm to evaluate the comparison between 2D- and 3D-sequences under the same condition.

In the phantom study, in line with our expectation, MR sialographic images using 3D-FSE with 0.5 mm slice thickness produced the best result in terms of conspicuity, production of virtual endoscopy, accurate representation of tube width, and C/N ratio in all sequences. This may be due to improvements in spatial resolution, C/N, SNR and accumulation of 3D-MR data using 3D-FSE sequences (Yang *et al*, 1999; Becker *et al*, 2000; Naganawa *et al*, 2001; Morimoto *et al*, 2002, in press). Thus, the only point of difference between images created using 3D-FSE with 0.5 mm slice thickness and those with 1.5 mm was accuracy of representing tube width. When using 3D-FSE with 0.5 mm slice thickness, however, the acquisition time is over 1 h for volunteers, and clinical application is not feasible. Therefore, a 1.5 mm slice thickness was used for volunteers.

In the volunteer study, MR sialographic images using 3D-FSE with a 1.5 mm slice thickness also produced the best result in terms of conspicuity, production of virtual endoscopy, and C/N ratio in all sequences in the nine cases with no moving artifacts despite a long acquisition time (over 30 min). This is superior or equal to that of previous studies on visualization of second and tertiary ducts (Varghese *et al*, 1999; Yang *et al*, 1999; Becker *et al*, 2000; Jager *et al*, 2000; Shojaku *et al*, 2000; Yousem *et al*, 2000; Sakamoto *et al*, 2001; Morimoto *et al*, 2002, in press). Evaluation of secondary and tertiary ducts is important and essential for diagnosing some salivary gland abnormalities, such as acute and chronic inflammation, cyst, tumor, or Sjögren syndrome. MR sialography using 3D-FSE sequences should be clinically applied for patients with salivary gland diseases, for whom closer investigation is needed (Murakami *et al*, 1998; Morimoto *et al*, 2002, in press). The disadvantages of 3D-FSE methods were description of many capillary blood vessels around parotid glands and a much longest acquisition time.

In 3D-FASE sequences, contrary to our expectation, MR sialographic images using 1.5 mm slice thickness produced a better result in terms of conspicuity, production of virtual endoscopy, and C/N ratio, although it produced an inferior accuracy of tube width than when using 0.5 mm in the phantom and volunteer studies. We see nothing unusual about such a contradiction in light of prominent differences between the phantom and volunteers, e.g. movement artifacts, metabolism, circulation, etc. One possible explanation might be that the SNR and data of the MR images using FASE sequences was much less than with FSE. In 3D-FASE sequences, the reduction of SNR might be more important than improvement of spatial resolution in parallel with the reduction in voxel size, in contrast to 3D-FSE sequence.

The acquisition time using 3D-FASE with 1.5 mm slice thickness was about 4.5 min, and it was associated with little deterioration of spatial resolution due to prominent moving, except for in one case. In the 3D-FSE, in contrast, MR sialographic images of six of the 15 volunteers showed greater deterioration than those with 3D-FASE because of prominent movement associated with the longest acquisition time of about 30 min. Therefore, results obtained using 3D-FASE in terms of mean visual score, production of virtual endoscopy, and C/N ratio were better than those with 3D-FSE in the volunteer study. In MR sialography, a little movement leads to deterioration of image quality resulting from the markedly thinner diameters of the ducts in parotid and submandibular glands. Therefore, the parameters obtained in the present 3D-FSE volunteer study would be difficult to apply for all patients with salivary gland diseases. Our results mentioned above indicate that MR sialography using 3D-FASE sequences can be applied for patients with salivary gland diseases in the initial MR examination, and that using 3D-FSE can be reserved for patients for whom a closer investigation is necessary, provided they are able to remain motionless for about 30 min.

For 2D-sequences with MR sialography, the single-section acquisition with thick sections might be more appropriate than sequential MS with thin sections followed by MIP reconstruction in the present study. MR sialography using single-section acquisition with thick sections was capable of visualizing the continuous progression of main ducts, but this was not possible using sequential MS followed by MIP reconstruction. Sequential MS followed by MIP reconstruction were more appropriate than other sequences for magnetic resonance cholangiopancreatography (MRCP) (Ichikawa *et al*, 1996; Yamashita *et al*, 1997; Irie *et al*, 1998). The factors underlying the different results obtained for MR sialography and MRCP might include the thinner diameter of the

salivary gland ducts than those of bile and pancreatic ducts. In addition, the salivary gland ducts were unaffected by respiratory movement, unlike in the abdomen. However, the disadvantage of single-section acquisition with thick sections would be that the 3D information related to the progression of ducts was not properly visualized by MR sialography using the single-section acquisition with thick sections. In addition, the virtual endoscopic view was not capable of producing MR data from a single-section acquisition with thick sections.

The producibility throughout almost the entire main ducts in MR virtual endoscopic views (Davis *et al*, 1996; Neri *et al*, 1997; Yang *et al*, 1999; Morimoto *et al*, 2002, in press) almost completely corresponded with the visual scores of the ducts for all four sequences for MR sialography in both the 3D model and volunteer studies, and reflected MR sialographic image quality more precisely. In a previous study, we described virtual endoscopy of salivary gland duct with MR sialography data set as a new approach for the parotid gland ducts (Morimoto *et al*, 2002, in press). Some disadvantages associated with MR virtual endoscopic views were reported, namely that it cannot be applied to visualization of very narrow or small structures (Morimoto *et al*, 2002, in press). We speculated that the present method might be an easy and appropriate method for determination of a suitable MR sialographic sequence.

MR sialographic images and virtual endoscopic views with 3D-FASE have also been applied to patients with various kinds of salivary gland diseases, as they were in the previous study (Morimoto *et al*, 2002, in press). The characteristic findings of each disease were accurately visualized by both MR sialographic images and virtual endoscopic views (Morimoto *et al*, 2002, in press). The acquisition time associated with MR sialography using 3D-FASE sequences was only about 4.5 min without patient load, and the images were sufficient for diagnosis of sialoadenitis in ducts. Therefore, 3D-FASE sequences may be useful for MR sialography.

Acknowledgements

This study was supported in part by grants from the Grant in Aid for Scientific Research from the Ministry of Education, Science, Sports and Culture of Japan, a grant-in-aid for scientific research from the alumni association of Kyushu Dental College, and a grant-in-aid for research and development from the Kitakyushu Medical and Engineering Cooperative Association, Kitakyushu, to YM.

References

Becker M, Marchal F, Becker CD *et al* (2000). Sialolithiasis and salivary ductal stenosis: Diagnostic accuracy of MR sialography with three-dimensional extended-phase conjugate-symmetry rapid spin-echo sequence. *Radiology* **217:** 347–358.

Davis CP, Ladd ME, Romanowski BJ *et al* (1996). Human aorta: preliminary results with virtual endoscopy based on three-dimensional MR imaging data sets. *Radiology* **198:** 573–578.

Fischbach R, Kugel H, Ernst S *et al* (1997). MR sialography: initial experience using a T2-weighted fast SE sequence. *J Comput Assist Tomogr* **21:** 826–830.

Hebert G, Ouimet-Oliva D, Nicolet V *et al* (1993). Imaging of the salivary gland. *Can Assoc Radiol J* **44:** 342–349.

Ichikawa T, Nitatori T, Hachiya J *et al* (1996). Breath-held MR choloangiopancreatography with half-averaged single shot hybrid rare acquisition with relaxation enhancement sequence: comparison of fast GRE and SE sequences. *J Comput Assist Tomogr* **20:** 798–802.

Irie H, Honda H, Tajima T *et al* (1998). Optimal MR cholangiopanreatographic sequence and its clinical application. *Radiology* **206:** 379–387.

Jager L, Menauer F, Holzknecht N *et al* (2000). Sialolithiasis: MR sialography of the submandibular duct-an alternative to conventional sialography and US? *Radiology* **217:** 665–671.

Lomas DJ, Carroll NR, Johnson G *et al* (1996). MR sialography. Work in progress. *Radiology* **200:** 129–133.

Mandelblatt SM, Braun IF, Davis PC *et al* (1987). Parotid masses: MR imaging. *Radiology* **163:** 411–414.

Morimoto Y, Tanaka T, Yoshioka I *et al* (2002). Virtual endoscopic view of salivary gland ducts using MR sialography data from three dimension fast asymmetric spin-echo (3D-FASE) sequences: a preliminary study. *Oral Dis* **8:** 268–274.

Morimoto Y, Tanaka T, Tominaga K *et al* (in press). Clinical application of MR sialographic 3D-reconstruction imaging and MR virtual endoscopy for salivary gland duct analysis. *J Oral Maxillofac Surg* **62:** 1237–45.

Murakami R, Baba Y, Baba T *et al* (1998). MR sialography using half-Fourier acquisition single-shot turbo spin-echo (HASTE) sequences. *Am J Neurodadiol* **19:** 959–961.

Naganawa S, Koshikawa T, Fukatsu H *et al* (2001). MR cisternography of the cerebellopontine angle: comparison of three-dimensional fast asymmetrical spin-echo and three-dimensional constructive interference in the steady-state sequences. *Am J Neuroradiol* **22:** 1179–1185.

Neri E, Caramella D, Falaschi F *et al* (1997). Virtual endoscopy of the aorta: segmentation artifacts with perspective surface rendering of spiral CT data sets. *Radiology* **205:** 262.

Sakamoto M, Sasano T, Higano S *et al* (2001). Evaluation of pulse sequences used for magnetic resonance sialography. *Dentomaxillofac Radiol* **30:** 276–284.

Shojaku H, Shojaku H, Shimizu M *et al* (2000). MR sialographic evaluation of sialectasia of Stensen's duct: comparison with X-ray sialography and ultrasonography. *Radiat Med* **18:** 143–145.

Tanaka T, Morimoto Y, Masumi S *et al* (2002). Utility of frequency-selective fat saturation T2-weighted MR images for the detection of joint effusion in the temporomandibular joint. *Dentomaxillofac Radiol* **31:** 305–312.

Teresi LM, Lufkin RB, Wortham DG *et al* (1987a). Parotid masses: MR imaging. *Radiology* **163:** 405–409.

Teresi LM, Kolin E, Lufkin RB *et al* (1987b). MR imaging of the intraparotid facial nerve: normal anatomy and pathology. *AJR Am J Roentgenol* **148:** 995–1000.

Thibauly F, Halimi P, Bely N *et al* (1993). Internal architecture of the parotid gland at MR imaging: facial nerve or ductal system? *Radiology* **188:** 701–704.

Varghese JC, Thornton F, Lucey BC *et al* (1999). A prospective comparative study of MR sialography and conventional sialography of salivary duct disease. *AJR Am J Roentgenol* **173:** 1497–1503.

Yamashita Y, Abe Y, Tang Y *et al* (1997). In vitro and clinical studies of image acquisition in breath-hold MR cholangiopancreatography: single-shot projection technique versus multislice technique. *Am J Roentgenol* **168:** 1449–1454.

Yang D, Kodama T, Tamura S *et al* (1999). Evaluation of the inner ear by 3D fast asymmetric spin echo (FASE) MR imaging: phantom and volunteer studies. *Magn Reson Imaging* **17:** 171–182.

Yousem DM, Kraut MA, Chalian AA (2000). Major salivary gland imaging. *Radiology* **216:** 19–29.

Zenk J, Hosemann WG, Iro H (1998a). Diameters of the main excretory ducts of the adult human submandibular and parotid gland: a histologic study. *Oral Surg Oral Med Oral Pathol* **85:** 576–580.

Zenk J, Zikarsky B, Horsemann WG *et al* (1998b). The diameter of the Stenon and Wharton ducts. Significance for diagnosis and therapy. *HNO* **46:** 980–985.